NASA TECHNICAL MEMORANDUM

NASA TM X-71568

NASA TM X-71568

FORMULATION OF A DISTORTION INDEX BASED ON PEAK COMPRESSOR PRESSURE RATIOS

by James E. Calogeras and Paul L. Burstadt
Lewis Research Center
Cleveland, Ohio 44135

TECHNICAL PAPER presented at Eleventh National Conference on Environmental Effects on Aircraft and Propulsion Systems
Trenton, New Jersey, May 21-23 1974

FORMULATION OF A DISTORTION INDEX BASED ON PEAK COMPRESSOR PRESSURE RATIOS

James E. Calogeras and Paul L. Burstadt
NASA-Lewis Research Center
Cleveland, Ohio

AUTOBIOGRAPHIES

Mr. Calogeras obtained his B.S. degree in Aeronautical Engineering from the University of Detroit in 1964 and his M.S.E. degree in Aerospace Engineering from the University of Michigan in 1967. Since 1964, Mr. Calogeras has worked in the Inlet Systems Section of the Wind Tunnel and Flight Division. During the past six years, he has specialized in inlet-engine compatibility problems related to dynamic distortions produced by supersonic inlets.

Mr. Burstadt received his B.S.E. (1968) and M.S.E. (1973) degrees in Aerospace Engineering from the University of Michigan. Since joining NASA-Lewis in 1969, Mr. Burstadt has worked in the Inlet Systems Section of the Wind Tunnel and Flight Division. He has been primarily involved with experimental investigations of inlet-engine compatibility problems of airbreathing propulsion systems.

ABSTRACT

In order to effectively use a compressor face total-pressure distortion index as a measure of inlet-engine compatibility, a correlation of distortion amplitude with stall margin must be developed with minimal scatter. A recent analysis of data recorded in extensive distortion screen tests with the J85-GE-13 turbojet engine has resulted in a correlation based on compressor discharge pressure ratioed to the minimum pressure at the compressor face. Simply by determining compressor stall lines with a single hub radial distortion pattern, a single tip radial pattern, and with undistorted inflow, the overall compressor pressure ratio at stall for even the most complex distortion pattern was found to be predictable.

1<

A simple compressor face distortion index has been formulated from these findings and has been applied to the data. This formulation represents a derivative of the parallel compressor theory. It is unique in its applicability to both radial and circumferential distortions, as well as combinations thereof.

INTRODUCTION

In 1969, an experimental investigation was made in the NASA-Lewis Research Center Propulsion Systems Laboratory (PSL) Altitude Chamber to determine the effect of screen-induced total pressure distortion on the stall margin of a J85-GE-13 turbojet engine. Results of this test are reported in reference 1 and summarized in table I of this report. An empirical distortion index was formulated from these results and applied to a set of time-variant distortion data recorded in the Lewis Research Center 10- by 10-foot Supersonic Wind Tunnel with an axisymmetric mixed-compression inlet coupled to the identical J-85 engine (refs. 2 through 4). These results were in part inconclusive, and it is now known that the empirical distortion index derived from the 1969 screen test results was not applicable to many of the instantaneous distortion patterns that were produced in the supersonic inlet.

A motion picture made from a continuous series of instantaneous pressure contours best illustrates the problem of describing a distorted flow that can change drastically in a fraction of a second. Frames from the film were made by digitizing time-variant data from each of 30 compressor face dynamic total pressure probes, (cf. fig. 1), at a rate of 8000 samples per second. Contours were formed, utilizing a computer graphics program, from combined steady-state and time-variant pressures. A sample of these contours is presented in figure 2. Here each shaded region represents a range of total pressure recovery, with the darkest regions corresponding to the lowest recovery. The boundary between any two shaded regions is then a constant pressure contour. The map on the left was made from steady-state pressures. It represents almost a pure hub radial distortion. The one on the right is an instantaneous distortion contour plot. This pattern has a large circumferential distortion component. If it is understood that the steady-state contour results from a combination of perhaps hundreds of the instantaneous contours, the problem in developing a distortion index that adequately describes all these patterns becomes more evident.

In order to obtain results for a wider range of distortion patterns, a second screen-induced distortion test was run in the PSL facility in 1972. This test used two J-85 engines other than the one run in 1969. Results of this test are reported in reference 5 and summarized in table II of this report. The scatter of the correlation of distortion amplitude versus loss in compressor pressure ratio at stall grew. In 1973, a second attempt at correlating the entire 1969/1972 composite data set was initiated. This attempt was based on an approach called DIDENT (an acronym for "Distortion Identity"). Results to date are contained herein.

E-8005

RESULTS AND DISCUSSION

Composite Data Set

A summary of the 1969/1972 composite data set is presented in figure 3. Parametric variations were made in the distortion intensity and the circumferential and/or radial extent of the spoiled area of many of these patterns. Compressor stalls were recorded at engine speeds ranging from 85- to 100-percent of rated engine speed. In all, 44 patterns and 176 stall points compose this data set. All of these points, with the exception of the full and partial midspan radial stall points, which had little or no effect on compressor performance or stability, were used in the DIDENT correlation.

Parallel Compressor Concept

The basis of the DIDENT approach, presented in figure 4, is the parallel compressor concept suggested by Pearson and McKenzie in reference 6. This theory divides a compressor subjected to pressure distorted inflow into parallel compressors, each with an undistorted inflow of different total pressure. It is assumed that each compressor operates on the same undistorted compressor speed characteristic, that there are no crossflows between compressors, and that the compressors discharge to a constant and uniform static pressure.

In the case of the J-85 engine, compressor discharge total pressure is quite uniform, even with a severely distorted inlet flow. For this reason, average measured compressor discharge total pressure rather than static pressure was used in this parallel compressor theory model and the development of DIDENT. Further, the low pressure at the compressure face, $(P_{min,\ 60^o})_{2,r}$, was defined as the lowest pressure, averaged over a 60^o circumferential sector, in a ring immediately adjacent to either the hub or tip circumference and consisting of 20-percent of the compressor face flow area. In practice, averaging over 60^o was only a consideration when the circumferential extent of the screen pattern was less than 60^o. This averaging accounts for a minimum blade residence time in which the compressor may react in a steady-state manner, (cf. ref. 1). The concept of critical angle is somewhat analogous to an overall reduced frequency parameter, as pointed out by Williams and Yost in reference 7. Only the hub and tip instrumentation rings (cf. fig. 1) were used to define the minimum pressure since it was reasoned that stall would originate at either the root or tip sections of the blade. This reasoning has been somewhat substantiated by the negligible effect of full and partial midspan radial distortions (cf. refs. 1 and 5).

In its simplest form, the parallel compressor concept predicts compressor stall when the compressor pressure ratio of any of the parallel compressors intersects the undistorted stall line. The accuracy of this prediction for circumferential distortion patterns is shown in the next figure.

In figure 5, the peak compressor pressure ratio at stall $\bar{P}_3/(P_{min,\ 60^o})_{2,r}$ is plotted as a function of corrected engine speed. The screen data represent all of the single and multiple per revolution circumferential distortions tested in the 1969 screen test. The solid curve is the undistorted stall line of the compressor.

3<

The correlation here is very good, and it is about as good with the 1972 screen patterns of the same type. So apparently, the main premise of the parallel compressor concept holds very well for the J-85 engine, at least with circumferential distortions.

This same type correlation is presented in figure 6. In this case, the parallel compressor concept was applied to full and partial hub radial distortion patterns from the 1969 data set. The solid curve is faired through the data, and the broken line is the undistorted stall line of the compressor. At the higher corrected speeds, the faired curve falls somewhat above the undistorted stall line. This same result was found with the 1972 data of this type. It probably means that, once the distorted flow is inside the compressor, a spanwise flow redistribution takes place which attenuates the distortion. The interesting point of this figure is that, with reasonable accuracy, the solid line could be obtained by testing just one of these patterns.

In figure 7, peak compressor pressure ratios at stall are presented for full and partial tip radial patterns run in the 1969 test. Results are similar to the case of full and partial hub radial distortion but they fall on a different faired curve. Again, within reasonable accuracy, this curve could have been obtained by testing a single tip radial pattern.

A comparison of peak stall compressor pressure ratio fairings from the 1969 test is made with corresponding fairings from the 1972 test in figure 8. Both the hub and particularly the tip regions of the 1972 engine produced more pressure ratio at stall than did the 1969 engine. As might be expected, this resulted in about a 3-percent higher overall pressure ratio at stall for the undistorted (or full span circumferential) characteristic.

Unfortunately, these curves show that a tight correlation for a particular J-85 engine requires testing that particular serial number engine. But the results seem to indicate that the test would only require running a single hub radial, a single tip radial, and either a single circumferential or an undistorted stall line. This could represent a large reduction in the amount of screen testing needed in the development cycle of an engine.

Distortion Identity

In order to formulate a distortion index that would be useful for isolated inlet testing, the data from the curves of figure 8 was expressed in terms of compressor face total pressures and correlated with loss in stall compressor pressure ratio (LSPR). To accomplish this, an identifier function was first defined. This function (K_i) is dependent on the basic distortion pattern, the serial number engine, and engine corrected speed. At a constant corrected speed, the identifier function K_i is simply the ratio of the regional to the undistorted stall pressure ratio, as shown in figure 8. Hence, for circumferential distortion, $K_i = 1.0$.

It was then possible to substitute the definition of the identifier function into the definition of LSPR to yield the distortion identity, DIDENT, as shown below:

Since

$$\text{LSPR} = \left\{1 - \frac{(\overline{P}_3/\overline{P}_2)_D}{(\overline{P}_3/\overline{P}_2)_U}\right\}_{N/\sqrt{\theta_2} = \text{const.}}$$

and

$$K_i = \left\{\frac{\left[\overline{P}_3/(P_{min,\ 60^o})_{2,r}\right]_D}{(\overline{P}_3/\overline{P}_2)_U}\right\}_{N/\sqrt{\theta_2} = \text{const.}} = f\ (\text{pattern, engine, } N/\sqrt{\theta_2})$$

then

$$\text{LSPR} = 1 - \frac{(P_{min,\ 60^o})_{2,r}}{\overline{P}_2} K_i = \text{DI}$$

LSPR and K_i are both defined in terms of overall compressor pressure ratios at a constant corrected speed. Although many loss-in-stall-margin terms are defined at a constant corrected weight flow, the constant corrected speed definition was used in this case because it provided a better correlation.

With $K_i = 1.0$ for circumferential distortions, DIDENT reduces to the same prediction offered in reference 7. In fact, figure 14 of reference 7 shows the good agreement between the circumferential distortion patterns run in the 1969 J-85 screen test with those from a series of rig tests run at Rolls-Royce and reported in reference 8.

The DIDENT correlation of the circumferential distortion patterns contained in the composite 1969/1972 J-85 data set is presented in figure 9. The solid line represents the distortion identity and the dashed lines represent a degree of scatter that was considered to be acceptable. The scatter of the open symbols about the theoretical line is due only to the original data scatter of the correlation presented in figure 5.

Figures 10 and 11, respectively, present the DIDENT correlation for most patterns contained in the 1969 and 1972 data sets. The full and partial midspan radial distortion patterns were omitted from these figures. The full and partial mid-span radial distortions were omitted because the present procedure of using hub and tip probes to define $(P_{min,\ 60^o})_{2,r}$ would generate small negative values of the distortion identity. This would in fact be quite accurate since the patterns did have measured values of LSPR that were zero or slightly negative. However, since the patterns had such a negligible effect on the stall line, they were ignored in this presentation. For the combined circumferential and partial radial distortion patterns and the instantaneous distortion pattern, values of K_i were determined from plots of the type shown in figures 5 through 7 included in reference 5.

Considering the simplicity of DIDENT, the correlation shown in these figures is very promising. Other than pattern numbers 1 and 10 in figure 11 (26.4% porosity screen), unacceptable scatter of most other stall points has been attributed to instrumentation inadequacies and interpolation errors.

E-8005

CONCLUDING REMARKS

The results presented demonstrate an approach to formulating a distortion descriptor (DIDENT) from a small number of classical distortion patterns. This descriptor uses a modified version of the parallel compressor concept to account for both radial and circumferential distortions. In this case the approach was applied to a turbojet engine with a single compression component. But there is nothing in the formulation or application of DIDENT that precludes its use for any type of turbine engine.

A summary of the present approach is as follows:

1. Determine critical angle θ_{crit} (or overall reduced frequency parameter) for circumferential distortions.

2. Plot curves of $\bar{P}_3/(P_{min}, \theta_{crit})_{2,r}$ for circumferential, hub-radial and tip-radial distortion patterns as functions of corrected engine speed. Determine K_i.

3. Determine engine-to-engine variations of K_i. If necessary, determine the undistorted stall line for each serial number engine, together with a single hub-radial and single tip-radial stall line for each engine.

4. Evaluate the distortion identity (DIDENT). The present approach makes use of the fact that there was no total pressure distortion at the compressor discharge. If this were not the case, P_3 would be replaced by p_3 —in the formulation of DIDENT.

Further work is planned to investigate the application of DIDENT to a multi-compressor turbine engine. A computer implementation of DIDENT is also planned that would be capable of evaluating a distortion pattern to determine whether the hub, tip, or circumferential identifier function, K_i, should be used. Such an implementation might use a series of radially averaged (i.e. rake average) pressures to identify circumferential distortions while retaining the use of hub and tip pressures to identify radial distortions. This implementation should be considered an integral part of the evaluation of DIDENT mentioned above in item 4.

NOMENCLATURE

A area, m^2 (ft^2)

DI distortion index, $1 - \dfrac{(P_{min,\ 60^\circ})_{2,r}}{\bar{P}_2} K_i$

K_i identifier function, defined in "Results and Discussion"

LSPR loss in stall compressor pressure ratio $\left\{1 - \dfrac{(\bar{P}_3/\bar{P}_2)_D}{(\bar{P}_3/\bar{P}_2)_U}\right\}_{\frac{N}{\sqrt{\theta_2}}} = \text{const.}$

E-8605

E-8005

M	Mach number
N	engine speed, rpm
N^*	rated engine speed, 16,500 rpm
$\frac{N \times 100}{N^* \sqrt{\theta_2}}$	corrected engine speed, percent
P	total pressure, N/m^2 (lbf/ft^2)
p	static pressure, N/m^2 (lbf/ft^2)
T	total temperature, K (^oR)
W	engine airflow, Kg/sec (lbm/sec)
$\frac{W\sqrt{\theta}}{\delta}$	corrected airflow, Kg/sec (lbm/sec)
β	extent of pressure below average, deg.
δ	local corrected total pressure, $P/101325 N/m^2$ ($P/2116 lbf/ft^2$)
θ	local corrected total temperature, T/288.2K ($T/518.7^oR$)
θ_{crit}	critical spoiled sector angle, degrees

Subscripts:

D	distorted inflow stall point
sp	spoiled or distorted
U	undistorted inflow stall point
1	mass flow measuring station
2	compressor face station
3	compressor discharge station
min,60^o	lowest mean value in a 60^o sector of station 2
r	inner or outer 20% area annulus of station 2

Superscripts:

	spatial average

REFERENCES

1. Calogeras, J. E.; Mehalic, C. M.; and Burstadt, P. L.: Experimental Investigation of the Effect of Screen-Induced Total-Pressure Distortion on Turbojet Stall Margin. NASA TM X-2239, 1971.

7<

2. Calogeras, J. E.; Burstadt, P. L.; and Coltrin, R. E.: Instantaneous and Dynamic Analysis of Inlet-Engine Compatibility. AIAA Paper 71-667, June, 1971.

3. Calogeras, J. E.: Instantaneous Distortion Investigation. NASA TM X-68189, 1972.

4. Burstadt, P. L.; and Calogeras, J. E.: Instantaneous Distortion in a Mach 2.5, 40-Percent-Internal-Contraction Inlet and its Effect on Turbojet Stall Margin. NASA TM X-3002, 1974.

5. Calogeras, J. E.; Johnsen, R. L.; and Burstadt, P. L.: The Effect of Screen-Induced Total-Pressure Distortion on Axial-Flow Compressor Stability. NASA TM X-3017, 1974.

6. Pearson, H; and McKenzie, A. B.: Wakes in Axial Compressors. J. Roy. Aeronautics Society, Vol. 63, No. 583, July, 1959, pp. 415-416.

7. Williams, D. D.; and Yost, J. O.: Some Aspects of Inlet/Engine Flow Compatibility. Aeronautics Journal, Vol. 77, No. 753, September, 1973, pp. 483-492.

8. Reid, C.: The Response of Axial Flow Compressors to Intake Flow Distortion. ASME Paper 69-GT-29, March, 1969.

E-8005

TABLE I. - SCREEN PATTERNS

1969 Test Program

Pattern	Type	Mesh	Wire diameter, in. (cm)	Porosity, percent open	Circumferential extent, deg	Spoiled area ratio, A_{sp}/A_2	Percent corrected speed, $\frac{N}{N^*\sqrt{\theta}} \times 100$	Screen pressure drop, $\frac{P_{min,2}}{\overline{P}_1}$	Distortion amplitude, $\left(\frac{P_{max} - P_{min}}{\overline{P}}\right)_2$	Remarks
1	Circumferential	$7\frac{1}{2}$	0.032 (0.081)	57.4	180	0.50	87.1	0.929	0.068	Stall point
							90.1	.914	.085	
							93.2	.898	.102	
							96.2	.874	.125	
							100.0	.851	.156	
2	Circumferential	$8\frac{1}{2}$	0.035 (0.089)	49.8	180	0.50	86.9	0.900	0.103	Stall point
							90.0	.882	.122	
							93.0	.861	.148	
							96.0	.834	.176	
							99.8	.802	.220	
3	Circumferential	9	0.041 (0.104)	39.7	180	0.50	93.0	0.808	0.196	Stall point
							100.1	.745	.274	Stall point
4	Circumferential	$7\frac{1}{2}$	0.032 (0.081)	57.4	90	0.25	87.0	0.932	0.066	Stall point
							93.0	.905	.091	
							100.0	.864	.126	
5	Circumferential	$8\frac{1}{2}$	0.035 (0.089)	49.8	90	0.25	87.0	0.918	0.080	Stall point
							89.9	.900	.097	
							92.9	.885	.112	
							95.9	.866	.129	
							99.7	.840	.159	
6	Circumferential	9	0.041 (0.104)	39.7	90	0.25	92.9	0.849	0.154	Stall point
							100.0	.792	.215	Stall point
7	Circumferential	$7\frac{1}{2}$	0.032 (0.081)	57.4	60	0.167	86.9	0.937	0.058	Stall point
							89.9	.984	.069	
							92.9	.912	.080	
							96.0	.895	.095	
							99.9	.870	.113	
8	Circumferential	$8\frac{1}{2}$	0.035 (0.089)	49.8	60	0.167	86.7	0.922	0.070	Stall point
							89.9	.910	.086	
							92.8	.894	.097	
							96.1	.872	.118	
							99.7	.848	.138	
9	Circumferential	9	0.041 (0.104)	39.7	60	0.167	87.3	0.900	0.094	Stall point
							92.9	.863	.133	
							99.8	.806	.189	
10	Circumferential	$8\frac{1}{2}$	0.035 (0.089)	49.8	30	0.083	87.0	0.937	0.078	Stall point
							90.1	.923	.095	
							93.2	.907	.114	
							96.2	.890	.135	
							100.3	.868	.161	
11	Circumferential (dual sectors)	$8\frac{1}{2}$	0.035 (0.089)	49.8	60	0.333	86.9	0.913	0.081	Minimum A_8; no stall
							93.0	.880	.110	Stall point
							99.7	.822	.171	Stall point
12	Hub radial	$7\frac{1}{2}$	0.032 (0.081)	57.4	360	0.20	87.0	0.942	0.055	Stall point
							92.9	.920	.076	
							99.9	.869	.126	
13	Hub radial	$7\frac{1}{2}$	0.032 (0.081)	57.4	360	0.40	86.9	0.940	0.055	Stall point
							92.9	.913	.080	
							99.8	.861	.130	

TABLE I. - Concluded.

Pattern	Type	Mesh	Wire diameter, in. (cm)	Porosity, percent open	Circumferential extent, deg	Spoiled area ratio, A_{sp}/A_2	Percent corrected speed, $\frac{N}{N^*\sqrt{\theta}} \times 100$	Screen pressure drop, $\frac{P_{min,2}}{\overline{P}_1}$	Distortion amplitude, $\left(\frac{P_{max} - P_{min}}{\overline{P}}\right)_2$	Remarks
14	Hub radial	9	0.041 (0.104)	39.7	360	0.20	87.1 90.2 93.0 96.0 99.9	0.909 .895 .876 .852 .810	0.087 .100 .118 .151 .189	Stall point ↓
15	Hub radial	9	0.041 (0.104)	39.7	360	0.40	87.4 90.2 93.5 96.0 100.1	0.887 .875 .853 .830 .777	0.110 .123 .146 .172 .233	Minimum A_8; no stall ↓
16	Midspan radial	$7\frac{1}{2}$	0.032 (0.081)	57.4	360	0.40	86.9 89.8 92.9 95.9 100.0	0.934 .922 .908 .882 .858	0.055 .065 .078 .099 .126	Stall point ↓
17	Tip radial	$7\frac{1}{2}$	0.032 (0.081)	57.4	360	0.15	87.1 90.2 93.0 96.1 100.1	0.943 .935 .924 .908 .888	0.053 .060 .070 .084 .098	Stall point ↓
18	Tip radial	$7\frac{1}{2}$	0.032 (0.081)	57.4	360	0.30	92.9 95.8 99.8	0.906 .887 .865	0.086 .107 .127	Stall point ↓
19	Tip radial	$7\frac{1}{2}$	0.032 (0.081)	57.4	360	0.60	87.0 90.8 92.8 95.7 99.6	0.921 .907 .895 .873 .848	0.073 .087 .096 .114 .141	Stall point ↓
20	Tip radial	$8\frac{1}{2}$	0.035 (0.089)	49.8	360	0.30	92.9 99.9	0.883 .837	0.115 .170	Stall point Stall point
21	Tip radial	$8\frac{1}{2}$	0.035 (0.089)	49.8	360	0.60	87.1 93.0 100.0	0.889 .850 .797	0.107 .148 .207	Stall point ↓
22	Graded tip radial	$8\frac{1}{2}$ (Outer ring) $7\frac{1}{2}$ (Inner ring)	0.035 (0.089) 0.032 (0.081)	49.8 57.4	360 360	0.30 0.30	87.1 93.1 96.0 99.9	0.893 .862 .834 .811	0.106 .137 .170 .195	Stall point ↓
23	Hub radial sector	9	0.041 (0.104)	39.7	120	0.067	87.1 90.0 93.0 96.1 100.0	0.912 .897 .881 .857 .825	0.080 .095 .109 .132 .161	Stall point ↓
24	Tip radial sector	9	0.041 (0.104)	39.7	120	0.133	87.1 90.0 92.9 96.0 99.9	0.903 .886 .869 .844 .817	0.095 .111 .131 .158 .186	Stall point ↓
25	Combined radial and circumferential	$7\frac{1}{2}$ (Hub radial) $8\frac{1}{2}$ (Circumferential)	0.032 (0.081) 0.035 (0.089)	57.4 49.8	270 90	0.15 .25	87.0 93.0 100.0	0.818 .887 .832	0.076 .107 .162	Stall point ↓
26	Combined radial and circumferential	$7\frac{1}{2}$ (Tip radial) $8\frac{1}{2}$ (Circumferential	0.032 (0.081) 0.032 (0.081)	57.4 57.4	270 90	0.45 .25	87.0 93.0 100.0	0.920 .887 .845	0.084 .124 .166	Stall point ↓

TABLE II. - SCREEN PATTERNS

1972 Test Program

Pattern	Type	Mesh number	Wire diameter, cm	Porosity, percent of open area	Circumferential extent, deg	Spoiled-area ratio, A_{SP}/A_2	Corrected engine speed, $\frac{N \times 100}{N^* \sqrt{\theta}}$, percent of rated	Pressure ratio, $\left(\overline{P}_{\text{min, 60°}}\right)_{2,s} \Big/ \overline{P}_1$	Average inlet total pressure, $\overline{P}_1$, N/m^2	Pressure ratio, $\overline{P}_2/\overline{P}_1$	Distortion, $\left[\left(1 - \frac{\overline{P}_{\text{min, 60°}}}{\overline{P}}\right)_r \sqrt{\frac{\theta_r}{\pi}}\right]_2$	Engine	Remarks
1	Circumferential	9	0.137	26.4	180	0.500	86.7	0.795	86 571	0.883	0.0991	A	Stall point
2	Circumferential	9	0.137	26.4	120	0.333	86.5	0.838	81 045	0.929	0.0772	A	Stall point
							92.8	.776	87 610	.902	.1108	A	Stall point
							96.8	.724	94 839	.879	.1400	A	Stall point
3	Circumferential	9	0.137	26.4	60	0.167	86.4	0.878	69 620	0.961	0.0495	A	Stall point
							89.5	.857	69 394	.955	.0583	↓	↓
							92.8	.834	69 268	.947	.0681		
							95.8	.803	69 795	.937	.0823		
							98.9	.771	69 863	.927	.0973	↓	
4	Instantaneous				~180		92.8	0.538	105 761	0.670	0.2015	B	Stall point (see RESULTS AND DISCUSSION
5	Instantaneous				~120		87.3	0.896	84 482	0.893	0.0478	A	T_5 limit - no stall
6	Circumferential	9	0.081	50.6	180	0.500	87.2	0.896	74 576	0.945	0.0428	A	Stall point
							92.8	.860	77 003	.924	.0596	A	↓
							98.5	.818	80 047	.899	.0803	A	
							87.2	.901	74 762	.946	.0386	B	
							93.2	.865	77 974	.921	.0579	B	
							98.5	.822	81 402	.896	.0769	B	↓
7	Circumferential	9	0.081	50.6	120	0.333	87.0	0.920	73 643	0.960	0.0342	A	Stall point
							92.9	.887	75 990	.944	.0485	A	Stall point
							98.2	.850	79 026	.927	.0667	A	Stall point
8	Circumferential	9	0.081	50.6	60	0.167	86.9	0.927	68 582	0.971	0.0270	A	Stall point
							93.0	.896	68 999	.980	.0375	A	Stall point
							98.1	.855	69 431	.946	.0548	A	Stall point
9	Circumferential	9	0.081	50.6	30	0.083	87.1	0.953	68 231	0.978	0.0144	A	Stall point
							93.0	.933	68 632	.968	.0208	A	Stall point
							98.1	.908	69 234	.957	.0284	A	Stall point
10	Hub radial	9	0.137	26.4	360	0.400	99.5	0.712	81 311	0.842	[a]0.1480	A	Stall point (engine failed)
							87.2	.833	74 722	.908	[a].0789	B	Stall point
							92.9	.786	76 966	.881	[a].1025	↓	↓
							96.1	.795	78 853	.863	[a].1215		
							98.8	.726	79 250	.850	[a].1408	↓	
11	Circumferential (2/rev)	9	0.081	50.6	2/90	0.500	87.0	0.909	73 372	0.948	0.0234	A	Stall point
							88.8	.900	76 486	.943	.0266	↓	↓
							92.4	.880	77 275	.931	.0321		
							98.0	.838	80 884	.906	.0463	↓	
12	Circumferential (2/rev)	9	0.081	50.6	2/45	0.250	86.9	0.938	74 212	0.967	0.0171	A	Stall point
							92.8	.917	78 943	.955	.0221	A	Stall point
							98.9	.871	81 819	.933	.0327	A	Stall point
13	Circumferential (2/rev)	9	0.081	50.6	2/30	0.167	87.3	0.955	73 742	0.972	0.0109	B	Stall point
							92.9	.937	76 222	.961	.0154	B	Stall point
							98.5	.907	79 558	.945	.0210	B	Stall point
14	Circumferential (4/rev)	9	0.081	50.6	4/30	0.333	86.9	0.943	73 153	0.962	0.0058	B	Stall point
							93.0	.929	76 892	.945	.0085	B	Stall point
							98.6	.887	81 554	.922	.0125	B	Stall point

TABLE II. - Concluded.

15	Combined radial and circumferential (2/rev)	9 (Partial tip)	0.081	50.6	2/90	0.100	87.1	0.922	71 932	0.976	0.0145	B	Stall point
		$\frac{\pi}{2}$ (circumferential)	.081	57.4	2/20	.089	92.7	.897	73 804	.963	.0204	B	Stall point
							98.8	.844	79 057	.945	.0340	B	Stall point
16	Partial tip radial (4/rev)	9	0.081	50.6	4/30	0.133	86.9	0.942	70 957	0.974	0.0062	B	Stall point
							92.9	.925	71 030	.966	.0084	B	Stall point
							98.7	.894	72 307	.949	.0120	B	T_5 limit - no stall
17	Partial hub radial	9	0.104	39.7	120	0.113	86.9	0.906	69 433	0.974	0.0475	B	Stall point
							92.9	.873	69 469	.964	.0661	B	Stall point
							98.6	.832	69 920	.954	.0887	B	Stall point
18	Partial hub radial	9	0.104	39.7	120	0.067	86.9	0.905	70 294	0.970	0.0427	B	Stall point
							92.9	.869	71 452	.959	.0596	B	Stall point
							98.4	.824	72 973	.946	.0845	B	Stall point
19	Partial hub radial	9	0.104	39.7	60	0.057	86.8	0.909	68 209	0.976	0.0363	B	Stall point
							92.8	.874	68 793	.967	.0509	B	Stall point
							98.5	.830	68 603	.956	.0710	B	Stall point
21	Partial hub radial	9	0.104	39.7	30	0.028	86.7	0.947	68 885	0.979	0.0174	B	Stall point
							92.5	.926	68 943	.971	.0242	B	Stall point
							97.7	.903	69 163	.982	.0323	B	Stall point
23	Partial tip radial	9	0.104	39.7	120	0.133	86.9	0.902	71 020	0.969	0.0377	B	Stall point
							92.9	.869	72 542	.956	.0536	B	Stall point
							98.5	.822	74 568	.943	.0771	B	Stall point
24	Partial tip radial	9	0.104	39.7	120	0.067	87.2	0.917	68 806	0.977	0.0311	B	Stall point
							92.9	.884	------	-----	.0443	B	Data recording no good
							98.3	.854	69 874	.958	.0566	B	Stall point
25	Partial tip radial	9	0.104	39.7	60	0.067	87.0	0.911	69 505	0.976	0.0294	B	Stall point
							92.9	-----	69 763	.962	.0510	B	Stall point
							98.7	.831	69 633	.953	.0598	B	Stall point
29	Mid-span partial radial	9	0.104	39.7	120	0.087	86.6	0.914	74 081	0.973	0.0432	B	Stall point
							92.6	.885	76 794	.964	.0583	B	Stall point
							97.8	.840	80 766	.948	.0811	B	Stall point
30	Combined patterns 10 and 23	9 (Hub radial)	0.137	26.4	360	0.400	87.0	0.933	74 218	0.896	0.0620	B	Stall point
		9 (Partial tip radial)	.104	39.7	120	.133	92.8	.911	76 990	.861	.0850	B	Stall point
							98.4	.881	80 824	.816	.1195	B	Stall point
31	Hub radial	9	0.104	39.7	360	0.400	86.9	0.892	71 506	0.939	[a]0.0487	B	T_5 limit - no stall
							92.8	.857	72 570	.922	[a].0688	B	Stall point
							98.2	.795	73 513	.889	[a].1036	B	Stall point
32	Combined hub radial and partial tip radial	9 (Hub radial)	0.104	39.7	360	0.400	87.0	0.871	77 808	0.910	0.0578	B	Stall point
		9 (Partial tip radial	.104	39.7	120	.200	92.8	.838	80 864	.896	.0744	B	Stall point
							98.7	.766	80 435	.830	.1179	B	Stall point
33	Combined patterns 23 and 31	9 (Hub radial)	0.104	39.7	360	0.400	86.7	0.883	70 829	0.925	0.0516	B	Stall point
		9 (Partial tip radial)	.104	39.7	120	.133	92.6	.845	72 827	.900	.0704	B	Stall point
							97.9	.777	76 335	.858	.1077	B	Stall point

[a]DPR distortion definition (appendix B).

STEADY-STATE AND DYNAMIC PRESSURE INSTRUMENTATION

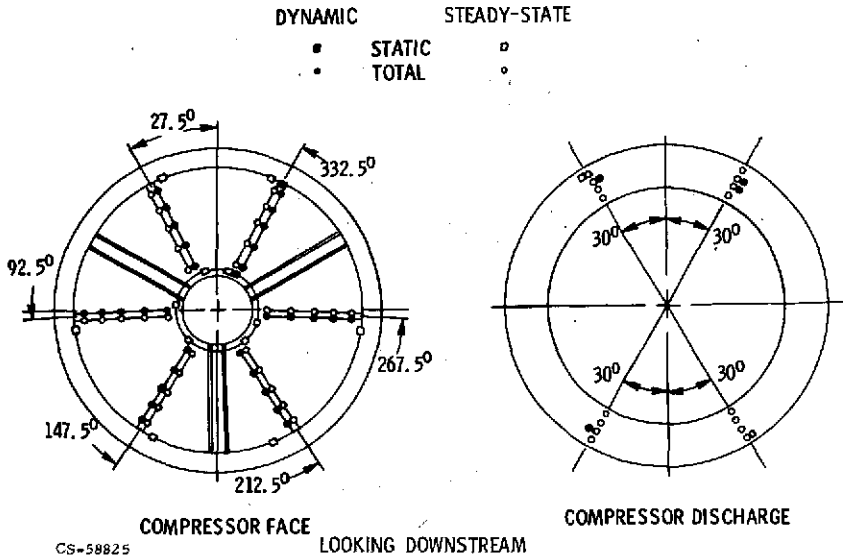

Figure 1.

DISTORTION CONTOURS

$\alpha = 0^0$ STALL POINT

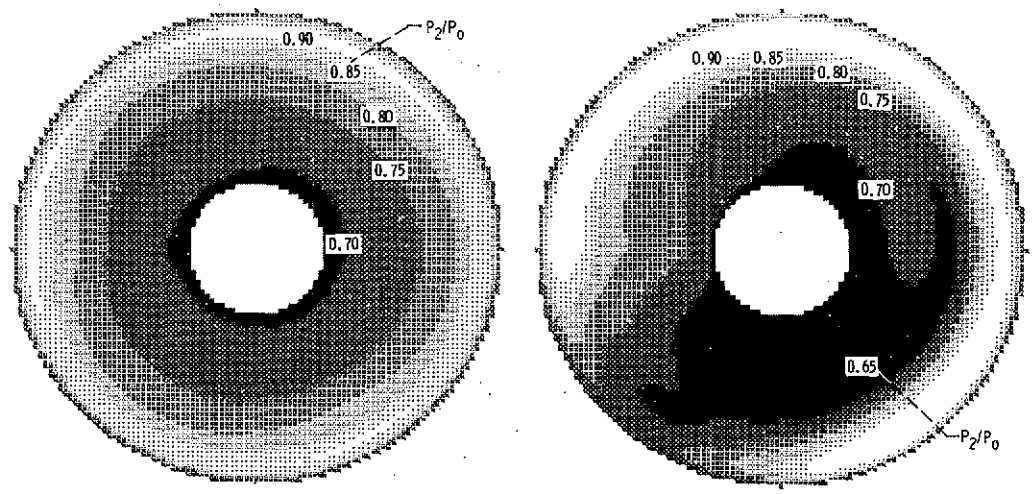

STEADY-STATE; $\overline{P}/P_0 = 0.788$

INSTANTANEOUS; TIME = 22.625 mSEC

Figure 2.

COMPOSITE DATA SET

J85-GE-13 SCREEN TESTS

PATTERNS, TYPE		TOTALS PATTERNS	TOTALS STALLS
CIRCUMFERENTIAL		18	76
RADIAL		12	49
PARTIAL RADIAL	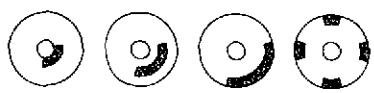	8	33
COMBINED		6	18

CS-70112

Figure 3.

PARALLEL COMPRESSOR CONCEPT

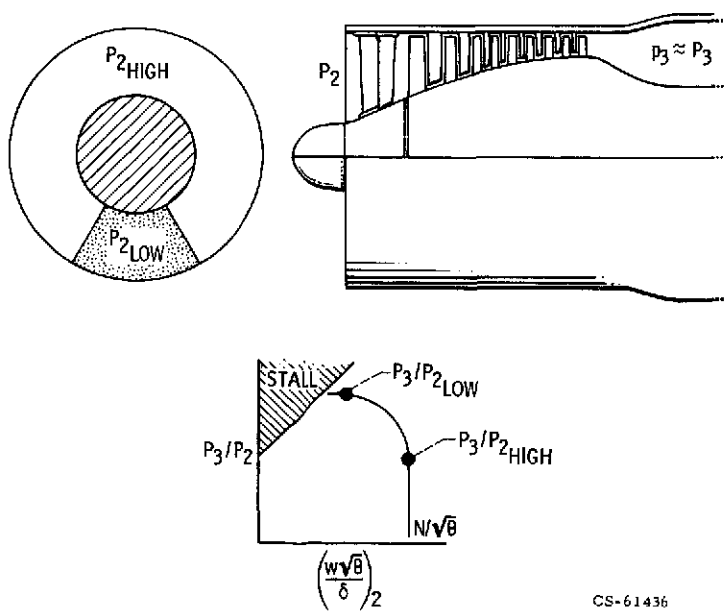

CS-61436

Figure 4.

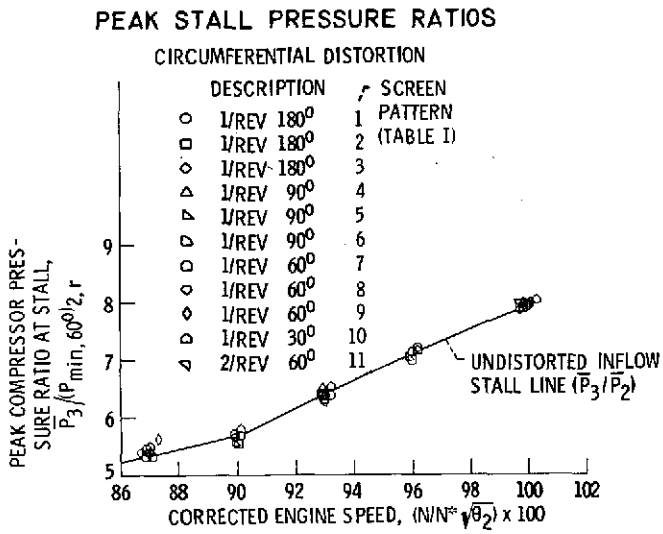

Figure 5. CS-70110

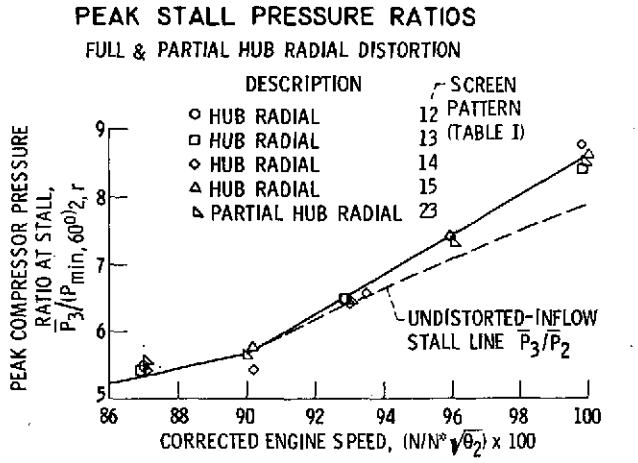

Figure 6. CS-70107

PEAK STALL PRESSURE RATIOS

FULL & PARTIAL TIP RADIAL DISTORTION

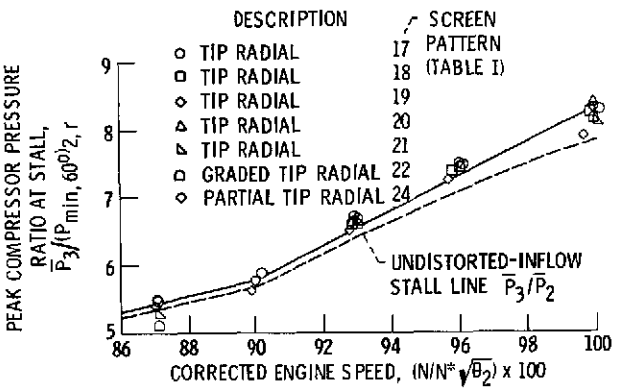

Figure 7. CS-70106

SUMMARY OF PEAK STALL PRESSURE RATIOS

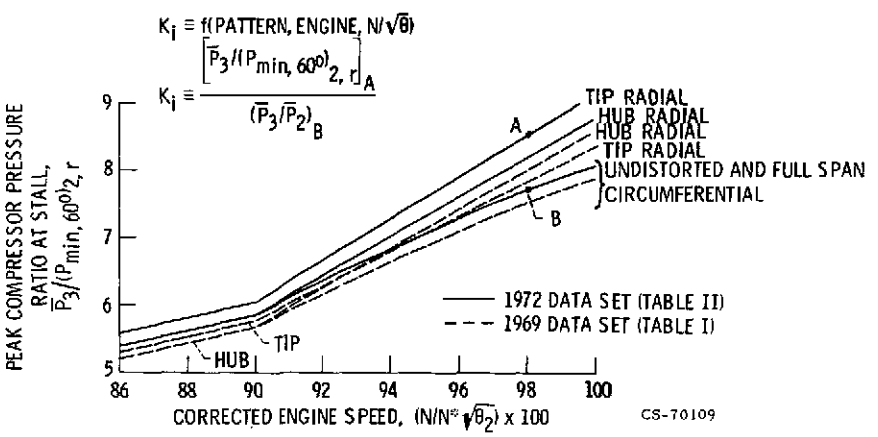

Figure 8.

CORRELATION OF CIRCUMFERENTIAL DISTORTION DATA

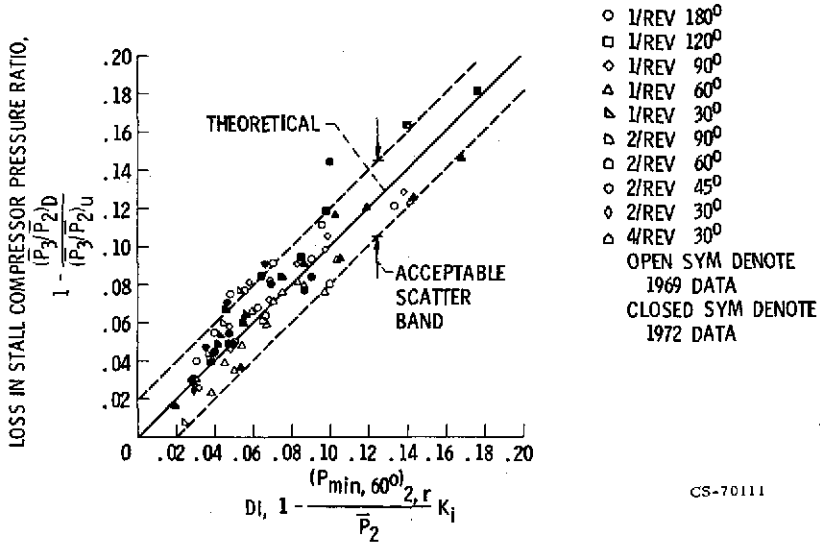

Figure 9.

CORRELATION OF 1969 DISTORTION DATA SET

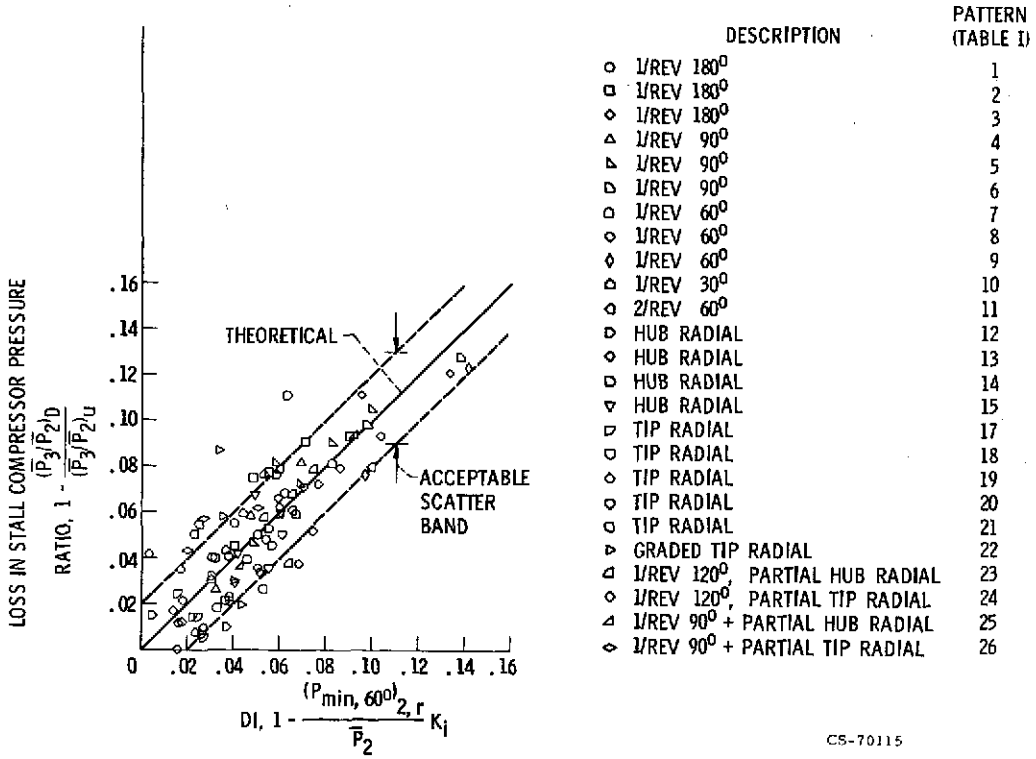

Figure 10.

CORRELATION OF 1972 DISTORTION DATA SET

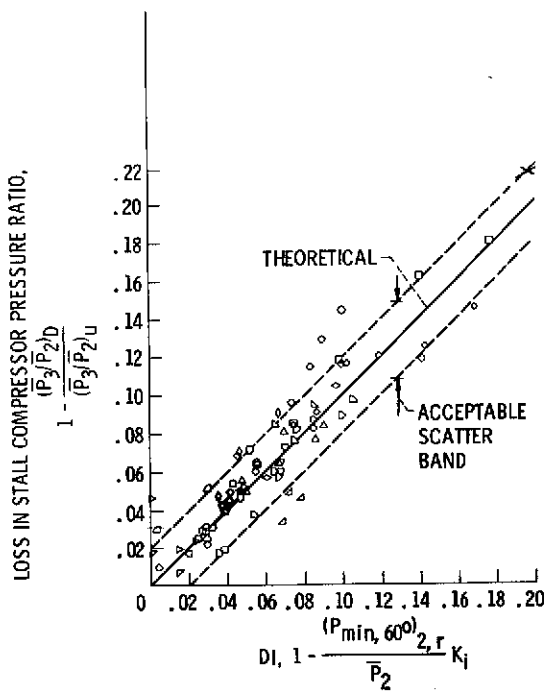

	DESCRIPTION	PATTERN (TABLE II)
○	1/REV 180°	1
□	1/REV 120°	2
◇	1/REV 60°	3
△	1/REV 180°	6
▷	1/REV 120°	7
▷	1/REV 60°	8
▷	1/REV 30°	9
◇	HUB RADIAL	10
○	2/REV 90°	11
◇	2/REV 45°	12
△	2/REV 30°	13
◁	4/REV 30°	14
▷	2/REV 20° + PARTIAL TIP RADIAL	15
▽	4/REV 30°, PARTIAL TIP RADIAL	16
▽	1/REV 120°, PARTIAL HUB RADIAL	17
▽	1/REV 120°, PARTIAL HUB RADIAL	18
◁	1/REV 60°, PARTIAL HUB RADIAL	19
△	1/REV 30°, PARTIAL HUB RADIAL	21
▷	1/REV 120°, PARTIAL TIP RADIAL	23
○	1/REV 120°, PARTIAL TIP RADIAL	24
▷	1/REV 60°, PARTIAL TIP RADIAL	25
▽	HUB RADIAL	31
○	COMBINED HUB RADIAL &	30
▷	1/REV 120°, PARTIAL TIP RADIAL	32, 33
×	INSTANTANEOUS	4

CS-70114

Figure 11.